Journal of Orthopaedic Translation 52 (2025) 138–149

Contents lists available at ScienceDirect

Journal of Orthopaedic Translation

journal homepage: www.journals.elsevier.com/journal-of-orthopaedic-translation

Original Article

# Application of biphasic mineralized collagen/polycaprolactone scaffolds in the repair of large load-bearing bone defects: A study in a sheep model

Meng-Xuan Yao [a,b,c,1], Jing-Chuan Zheng [d,1], Hai-Cheng Wang [e,1], Hong-Zhi Lv [a,b,c], Yi-Fan Zhang [a,b,c], Yu-Qin Zhang [a,b,c], Tai-Long Shi [a,b,c], Yan-Ze Zhu [f], Ying-Ze Zhang [a,b,c], Xiu-Mei Wang [d,*], Wei Chen [a,b,c,**]

[a] Department of Orthopaedic Surgery, Third Hospital of Hebei Medical University, Shijiazhuang, Hebei, 050051, People's Republic of China
[b] Key Laboratory of Biomechanics of Hebei Province, Shijiazhuang, Hebei, 050051, People's Republic of China
[c] NHC Key Laboratory of Intelligent Orthopaedic Equipment, Shijiazhuang, Hebei, 050051, People's Republic of China
[d] State Key Laboratory of New Ceramics and Fine Processing, Key Laboratory of Advanced Materials of Ministry of Education, School of Materials Science and Engineering, Tsinghua University, Beijing, 100084, People's Republic of China
[e] Hebei Key Laboratory of Integrated Traditional and Western Medicine in Osteoarthrosis Research (Preparing), Cangzhou Hospital of Integrated Traditional Chinese and Western Medicine in Hebei Province, People's Republic of China
[f] Beijing Allgens Medical Science and Technology Co., Ltd., Beijing, 102629, People's Republic of China

ARTICLE INFO

*Keywords:*
Biphasic mineralized collagen/polycaprolactone
bMC/PCL scaffolds
Bone healing
Femoral defect repair
Sheep model
Tissue engineering

ABSTRACT

*Objective:* This study aims to evaluate the efficacy of biphasic mineralized collagen/polycaprolactone (bMC/PCL) scaffolds in repairing large load-bearing bone defects, particularly femoral defects, using a sheep model.

*Methods:* The bMC/PCL scaffolds were prepared by combining porous mineralized collagen/polycaprolactone (pMC/PCL) with compact mineralized collagen/polycaprolactone (cMC/PCL). The scaffolds were characterized using scanning electron microscopy to observe the microstructure and compression testing to assess mechanical properties. Twenty female sheep were selected to create a 20 mm femoral defect model, divided into a blank group (no material implanted) and an experimental group (bMC/PCL scaffolds implanted), with 10 sheep in each group. Bone healing and lower limb functional recovery were assessed at 1 month, 3 months, and 6 months postoperatively using Lane-Sandhu scores and visual analog scale scores for lameness. Additionally, bone repair progress was analyzed through X-ray, Micro-CT, and histological analyses.

*Results:* Compared with the blank group, the bMC/PCL scaffold group showed significant improvement in bone defect repair. At 3 and 6 months postoperatively, X-ray, Micro-CT scans, and histological staining indicated stable scaffold integration and gradual new bone formation. The Lane-Sandhu scores in the experimental group were 3.60 ± 0.548 and 4.00 ± 0.707 at 3 and 6 months, respectively, whereas the blank group experienced plate/screw breakage leading to fixation failure, with scores of 1, indicating better bone healing in the experimental group. The lameness scores in the experimental group were 2.71 ± 0.97 and 1.48 ± 0.86 at 3 and 6 months, respectively, significantly lower than those in the blank group ($p < 0.0001$ and $p = 0.0002$). Micro-CT analysis showed that bone volume to tissue volume ratio increased from 28.07 ± 9.22 % to 62.02 ± 11.82 %, bone mineral density increased from 0.392 ± 0.032 g/cm$^3$ to 0.583 ± 0.125 g/cm$^3$, trabecular thickness increased from 0.690 ± 0.224 mm to 1.049 ± 0.089 mm, and trabecular separation decreased from 2.766 ± 1.183 mm to 0.501 ± 0.268 mm at 3 and 6 months postoperatively.

*Conclusion:* This study evaluated the efficacy of bMC/PCL scaffolds in repairing large load-bearing bone defects. The bMC/PCL scaffolds demonstrated good bioactivity and mechanical properties, indicating promising clinical

* Corresponding author.
** Corresponding author. Department of Orthopaedic Surgery, Third Hospital of Hebei Medical University, Key Laboratory of Biomechanics of Hebei Province, Shijiazhuang, Hebei, People's Republic of China 050051, NHC Key Laboratory of Intelligent Orthopaedic Equipment, Shijiazhuang, Hebei, 050051, People's Republic of China.
*E-mail addresses:* mengxuanyao@126.com (M.-X. Yao), zhengjingcc12@126.com (J.-C. Zheng), 15696472822@qq.com (H.-C. Wang), 190099199@qq.com (H.-Z. Lv), 15176139858@163.com (Y.-F. Zhang), zhangyuqinnm@163.com (Y.-Q. Zhang), 2435078994@qq.com (T.-L. Shi), zhuyanze1988@163.com (Y.-Z. Zhu), drzyzhangyingze@163.com (Y.-Z. Zhang), wxm@mail.tsinghua.edu.cn (X.-M. Wang), surgeonchenwei@126.com (W. Chen).
[1] Equal contribution (co-first authors).

https://doi.org/10.1016/j.jot.2025.03.014
Received 9 November 2024; Received in revised form 19 March 2025; Accepted 26 March 2025

application prospects. Future studies should further verify the safety and efficacy of these scaffolds in a wider range of animal models to support their clinical application.

*Significance statement:* The bMC/PCL scaffolds offer a promising solution for large femoral bone defects, with potential for clinical use in orthopedic and trauma surgeries.

*The translational potential of this article:* The application of bMC/PCL scaffolds in clinical practice is expected to significantly advance the treatment of large bone defects, particularly weight-bearing bone defects. The study shows that bMC/PCL scaffolds have a significant impact on the repair of large weight-bearing bone defects and functional recovery, indicating their potential for application in orthopedics and trauma care. Specifically, the material's supportive role in weight-bearing bones offers new possibilities for its use in the repair of weight-bearing bone defects. Furthermore, the performance of bMC/PCL scaffolds in bone healing makes them an ideal candidate material for treating various bone defects, with broad clinical application prospects. Further clinical trials are necessary to confirm their safety and efficacy in human patients.

## 1. Introduction

Globally, more than 20 million patients suffer from bone defects each year [1]. The primary causes of bone defects include trauma, tumors, infections, and congenital diseases, all of which profoundly impact patients' health and quality of life [2,3]. Therefore, bone defect repair holds significant importance in the medical field. Traditional treatment methods mainly involve the use of autografts and allografts, but the outcomes are not always ideal [4,5]. Although autografts can provide an excellent microenvironment for new bone formation and reconstruction, they come with complications at the donor site, limited donor supply, and potential pain issues [5–8]. Allografts, on the other hand, may pose risks of immune reactions and disease transmission [4]. To overcome these challenges, the development of novel biomaterials based on biomimetic strategies for bone regeneration has gradually become a research focus in the field of bone defect repair [1,9,10].

These novel biomaterials aim to mimic the extracellular matrix of bone, such as mineralized collagen, to enhance their bioactivity and biocompatibility [11–14]. Due to its excellent biocompatibility, osteoinductivity, and mechanical properties, mineralized collagen has gained extensive attention in bone defect repair [15,16]. The mineralized collagen (MC)/polycaprolactone (PCL) composite scaffold is one such material. MC is a naturally occurring material with good affinity for bone tissue, while PCL is a biodegradable material that has been widely used in clinical settings [17,18]. The combination of these two materials aims to achieve rapid and effective repair of large bone defects by leveraging the bioactivity of collagen and the mechanical strength of polycaprolactone.

In previous research, biphasic MC/PCL (bMC/PCL) scaffolds, composed of porous MC/PCL (pMC/PCL) scaffolds and compact MC/PCL (cMC/PCL) scaffolds, have demonstrated promising results in the repair of large cranial defects [19]. The cMC/PCL scaffold, due to its compact microstructure, possesses relatively high compressive strength and elastic modulus ($\sigma = 29.56 \pm 1.23$ MPa, $E = 3.17 \pm 0.39$ GPa), whereas the pMC/PCL scaffold exhibits weaker mechanical properties ($\sigma = 0.86 \pm 0.01$ MPa, $E = 0.05 \pm 0.01$ GPa). As a composite of these two materials, the bMC/PCL scaffold has mechanical properties that fall between those of pMC/PCL and cMC/PCL ($\sigma = 18.35 \pm 0.64$ MPa, $E = 1.13 \pm 0.03$ GPa). This allows the bMC/PCL scaffold to retain the bioactivity of the pMC/PCL scaffold while also providing the strength of the cMC/PCL scaffold, presenting a highly potential new material for cranial defect repair.

However, despite the promising performance of bMC/PCL scaffolds in large cranial defect repairs, their applicability in different types and scales of bone defects has not been considered. Load-bearing is crucial for bone formation, as described in classic literature [20,21], but many studies on tissue-engineered bone regeneration have been conducted in non-load-bearing sites [22–24]. Moreover, the potential application of bMC/PCL scaffolds in load-bearing bone defects, particularly in femoral defects, has not been systematically evaluated. This research gap not only limits the comprehensive understanding of this novel biomaterial but also potentially delays its broader clinical application.

Based on this research gap, we designed this study to comprehensively evaluate the application of bMC/PCL scaffolds in the repair of large femoral bone defects, aiming to fill this gap in the existing literature. We hypothesize that bMC/PCL scaffolds may also be suitable for the repair of large load-bearing bone defects, such as those in the femur, with mechanical properties sufficient to provide mechanical support to the weight-bearing bone before new bone formation. We selected sheep as the experimental animals and created large femoral bone defect models to compare the effectiveness of bMC/PCL scaffolds with traditional bone plates in bone defect repair. The study results reveal the potential of bMC/PCL scaffolds in the repair of large load-bearing bone defects, such as the femur, laying the foundation for their further clinical application.

## 2. Materials and methods

### 2.1. Preparation of different structured MC scaffolds

The preparation of MC powder followed the process described in our previous work [25], and together with PCL (Jinan Daigang Biomaterial Co., biomedical grade, 300 kDa), three types of scaffolds were constructed: pMC/PCL scaffolds, cMC/PCL scaffolds, and bMC/PCL scaffolds. The preparation methods for pMC/PCL and cMC/PCL scaffolds were referenced from previous literature [26–28]. The preparation of bMC/PCL scaffolds is illustrated in Fig. 1.

First, PCL powder was dissolved in 1,4-dioxane at a concentration of 0.1 g/ml. Then, MC powder at 0.1 g/ml was added to form a homogeneous slurry. The slurry was then poured into a designed mold to create the pMC/PCL scaffold. After freezing at −20 °C, the precursor scaffold was freeze-dried to remove the solvent, resulting in the pMC/PCL scaffold. PCL powder was melted and mixed with MC powder at a 1:1 ratio, then pressed into shape under 30 MPa pressure for 10 min, followed by air cooling to obtain scaffolds with a diameter of 15 mm and a height of 20 mm. The preparation of bMC/PCL scaffolds was based on the aforementioned procedures. First, a cMC/PCL scaffold with a diameter of 15 mm and a height of 20 mm was prepared, then embedded into the pMC/PCL precursor slurry and freeze-dried. Finally, all scaffolds were sterilized by 60Co irradiation and stored under sterile conditions for further use.

### 2.2. Characterization of scaffold physical properties

The microstructure of the scaffolds was observed using a scanning electron microscope (SEM) (GEMINI SEM, Zeiss, Germany). To maintain the natural state of the internal pore structure, the samples were subjected to ultra-low temperature treatment in liquid nitrogen and then quickly fractured to obtain fresh cross-sections. Prior to observation, a platinum layer with a thickness of 5–10 nm was sputtered onto the sample surfaces.

The compressive strength and elastic modulus of the pMC/PCL, cMC/PCL, and bMC/PCL scaffolds were measured using a universal mechanical testing machine (SHIMADZU AG-IC, Japan) with a 2000 N

load sensor. Samples were prepared as standard cylinders with a diameter of 10 mm and a length of 20 mm. Load was applied to the scaffolds until they reached 30 % of their original length. The compressive modulus was calculated from the slope of the initial linear portion of the stress–strain curve. Compressive strength was determined from the intersection of the stress–strain curve at the 20 % strain point with a line having the same slope as the elastic modulus. Three independent measurements were performed for each group to conduct statistical analysis.

Since the cMC/PCL scaffold primarily serves as a mechanical support component, we only evaluated the porosity of the pMC/PCL scaffold. The porosity was measured using the liquid displacement method. Cylindrical pMC/PCL samples of known dimensions were prepared using a custom mold, and the volume of each sample (V1) was calculated based on its geometric dimensions. The dry mass of each sample was recorded as m1. Subsequently, the samples were immersed in a vacuum filtration bottle filled with ultrapure water to create a closed system. A vacuum pump was used to extract air from the bottle, generating a pressure gradient that forced water into the scaffold's pores. When no more bubbles were observed escaping, it indicated that the scaffold pores were completely filled with water. The sample was then carefully removed, and surface moisture was gently wiped off with filter paper. The mass of the water-saturated sample was recorded as m2. The mass of the water within the pores (m3) was calculated as follows:

$$m3 = m2 - m1$$

The volume of this water (V2) corresponds to the total pore volume of the scaffold, calculated as:

$$V2 = \frac{m3}{\rho_{water}}$$

Where $\rho_{water}$ represents the density of water at room temperature. Finally, the porosity of the scaffold was determined using the following formula:

$$Porosity(\%) = \frac{V2}{V1} \times 100\%$$

### 2.3. In vivo evaluation of bMC/PCL scaffolds in sheep femoral defect model

All animal experimental procedures were conducted in accordance with the guidelines for the care and use of laboratory animals provided by the Ministry of Public Health of China and the National Institutes of Health (NIH) of the United States, following the directives of the Institutional Animal Care and Use Committee (IACUC).

We used a large femoral defect model to evaluate the performance of bMC/PCL scaffolds in sheep. Twenty healthy, non-pregnant adult female sheep, weighing between 50 and 70 kg, were selected and randomly divided into two groups: the defect group without material implantation (blank group) and the bMC/PCL scaffold implantation group (experimental group).

After administering an injection of 3 % pentobarbital sodium (30 mg/kg body weight), the anesthetized animals were placed in a lateral position on the operating table, and their forelimbs were secured. The surgical site on the sheep was shaved, and an incision was made to expose the femur. Under fluoroscopic guidance, a Kirschner wire was inserted to determine the osteotomy site. A sagittal saw was used to perform the osteotomy perpendicular to the femoral long axis, creating a bone defect of 2 cm in length. Once the model was successfully created, the treatments were applied according to the group assignments: the experimental group received bMC/PCL scaffold implantation at the defect site, while the blank group remained empty and the femur was fixed using bone plates. Finally, the wound was irrigated with saline and sutured (as shown in Fig. 2).

### 2.4. X-ray examination

At 1 month, 3 months, and 6 months post-surgery, both groups of sheep underwent X-ray examinations to assess the progress of bone defect repair. The Lane-Sandhu scoring system [29] was used to evaluate the repair status of the bone defects, with the specific scoring criteria as follows: Grade 1: No healing; Grade 2: Inconspicuous callus formation; Grade 3: Partial bridging of the bone defect; Grade 4: Gradual absorption of the bone callus at the defect site; Grade 5: Complete healing.

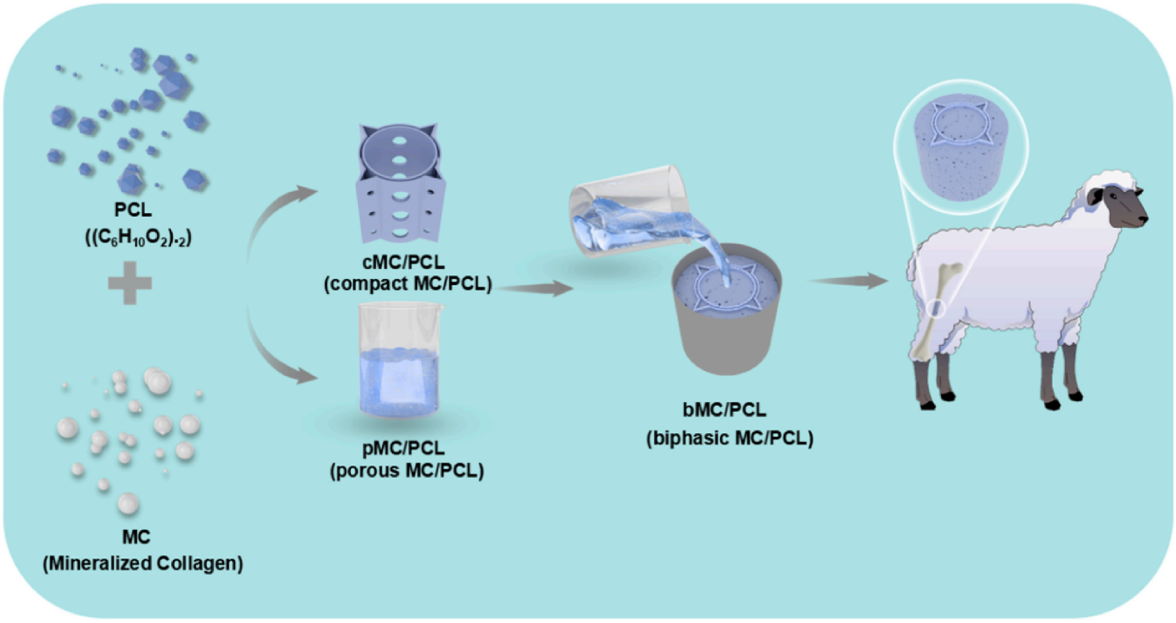


**Fig. 1.** Schematic diagram of the preparation and in vivo evaluation of bMC/PCL scaffolds. The bMC/PCL scaffold was constructed using melting-pressing and freeze-drying techniques. The cMC/PCL was made by melt-pressing PCL and MC, while the pMC/PCL was created by freeze-drying an organic solution of PCL and MC. The porous and compact parts were then organically combined to form the bMC/PCL. After implantation into a 20 mm femoral defect in sheep, the scaffold promoted the repair of the bone defect and the formation of new bone, ensuring the structural stability of the long-term repair area.

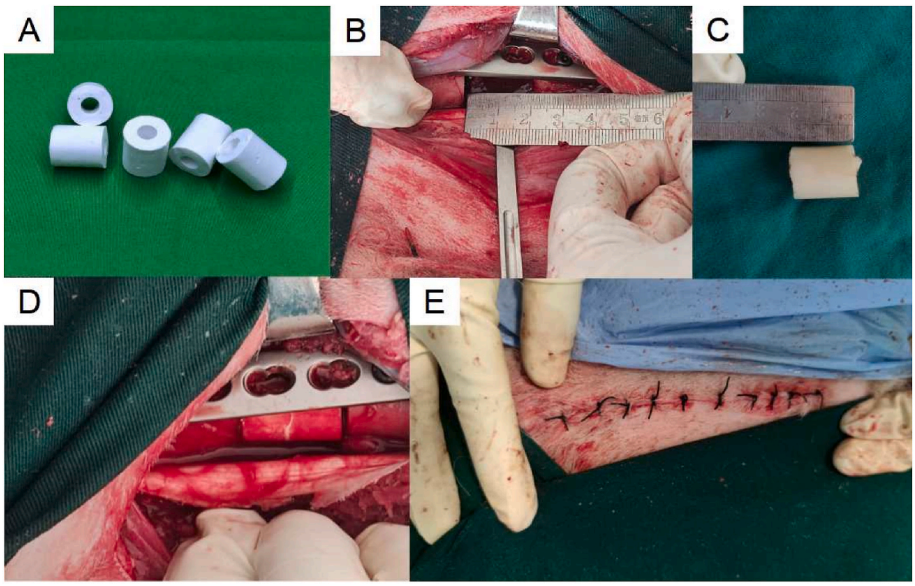


**Fig. 2.** Large femoral defect and the implantation process of the bMC/PCL scaffold. (A) The bMC/PCL scaffold. (B) The bone defect site in the control group left empty. (C) During the preparation of the bone defect, a 2 cm segment of the femoral cortical bone is removed. (D) The bMC/PCL scaffold implanted into the femoral defect in the experimental group. (E) The wound sutured after the surgery.

### 2.5. Lameness assessment

The lameness of the sheep was evaluated before surgery and at 1 month, 3 months, and 6 months post-surgery. The assessment used the Visual Analog Scale (VAS), which consists of a 100 mm continuous line with vertical markings. One end of the line is labeled "No lameness" (left side) and the other end is labeled "Most severe lameness" (right side) [30]. During the evaluation, the sheep were observed while trotting in a straight line and turning to the left and right. The observer marked the point on the line that best reflected the perceived degree of lameness based on the observation.

### 2.6. Micro-CT image analysis

At 3 months and 6 months post-surgery, the sheep were euthanized, and femoral samples were collected for Micro-CT examination (SKYScan 1176, Germany) to study bone formation. The scanning parameters were set to a current of 313 μA, a voltage of 80 kV, and an image pixel size of 30 μm. The collected data were used to reconstruct three-dimensional tomographic images and measure and calculate bone-related parameters using the accompanying software: bone mineral density (BMD), bone volume to tissue volume ratio (BV/TV), trabecular separation (Tb.Sp), and trabecular thickness (Tb.Th).

### 2.7. Histomorphological examination

The collected samples were fixed in 4 % paraformaldehyde for 2 weeks, followed by running water rinsing for 24 h. Subsequently, the samples were dehydrated in a gradient alcohol series (70 %–95 %). The samples were then soaked in the following solutions: anhydrous ethanol + Technovit 7200 resin solution (3:7) for 2 days, anhydrous ethanol + Technovit 7200 resin solution (1:1) for 2 days, Technovit 7200 resin solution I for 7 days, and Technovit 7200 resin solution II for 3 days. After embedding and polymerizing the samples in a light-curing machine, the samples were cut into 200 μm thick slices using a German EXAKT 300CP hard tissue microtome and ground using a German EXAKT 400S grinding machine. The slices were ground to 20 μm thickness using 320, 800, and 1200 grit sandpapers and polished with 4000 grit sandpaper before staining. Hematoxylin and eosin (HE) and Masson's trichrome stains were used to observe the bone tissue repair.

### 2.8. Nanoindentation experiment

The nanoindentation experiment was performed using a Nano Indenter XP (MTS Nano Instruments Inc., Oak Ridge, Tennessee, USA) to assess mechanical properties. A Berkovich indenter with a tip radius of 100 nm was used in the Continuous Stiffness Measurement (CSM) mode to measure the variations in hardness and Young's modulus as a function of indentation depth. The experimental samples were taken from the sheep femoral defect sites at 3 and 6 months after bMC/PCL implantation. The samples underwent low-speed cutting, embedding, grinding, and polishing to obtain a testing area with low surface roughness (Ra $<$50 nm). Six test points were selected in both the newly formed bone region and the native bone region. The maximum load was set to 20 mN, with a loading rate of 2 mN/s and a hold time of 10 s. The CSM frequency was set to 45 Hz to improve measurement accuracy. A total of six indentation tests were conducted, and the hardness and Young's modulus values were calculated based on the Oliver–Pharr method.

### 2.9. Statistical analysis

The results are expressed as the mean ± standard error. Data from the blank control group and the bMC/PCL scaffold group were compared using a one-way analysis of variance (ANOVA), followed by the least significant difference (LSD) post hoc test. For comparisons between two groups, a t-test was used. Statistical analyses were conducted using SPSS software (version 23.0; SPSS, Chicago, IL, USA), with statistical significance set at $p < 0.05$.

## 3. Results

### 3.1. Scaffold preparation and characterization

All scaffolds were prepared as cylindrical structures with a diameter of 15 mm and a height of 20 mm, as shown in Fig. 2A. Fig. 3 displays the Micro-CT and SEM images of the scaffolds. Fig. 3A shows the Micro-CT image of the cMC/PCL scaffold. Due to the porous structure of the low-density pMC/PCL phase and the dense structure of the high-density cMC/PCL phase, the Micro-CT image of the bMC/PCL scaffold (Fig. 3B) presents different contrasts, with the brighter areas representing the cMC/PCL phase and the darker areas representing the pMC/

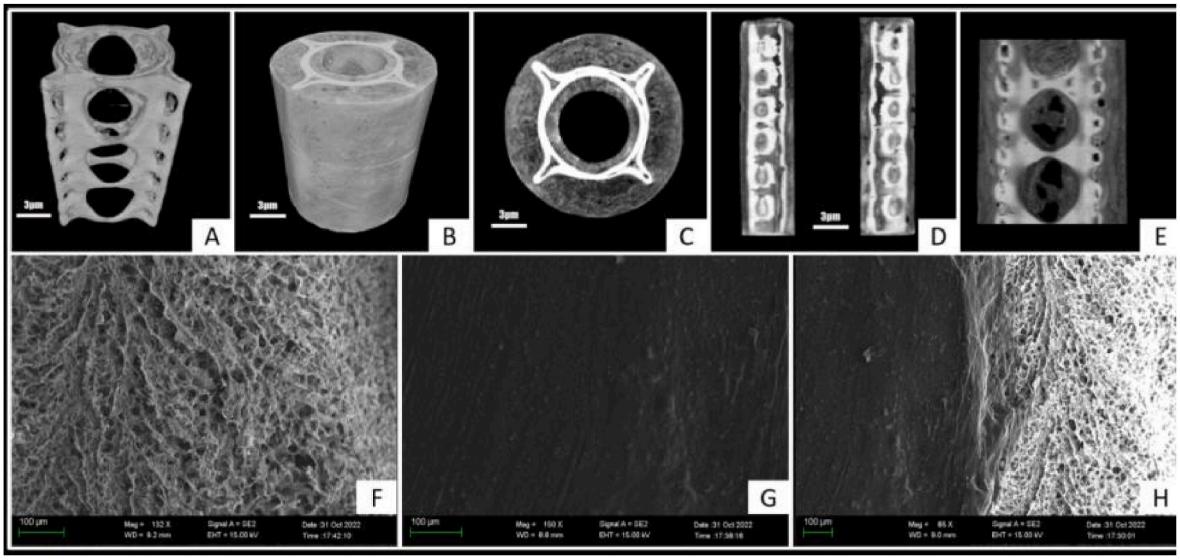


**Fig. 3.** Micro-CT and SEM images of the scaffolds. (A) Micro-CT image of the cMC/PCL scaffold. (B) Micro-CT image of the bMC/PCL scaffold, showing distinct contrasts due to the porous structure of the low-density pMC/PCL phase and the dense structure of the high-density cMC/PCL phase. The brighter areas represent the cMC/PCL phase, while the darker areas represent the pMC/PCL phase. (C–E) Cross-sectional images of the bMC/PCL scaffold in different directions, clearly displaying the internal porous structure and dense regions of the scaffold. (F) SEM image of the pMC/PCL scaffold, showing the typical interconnected and hierarchical pore structure. (G) SEM image of the cMC/PCL scaffold, displaying a compact morphology. (H) SEM image of the bMC/PCL scaffold, illustrating the interface bonding area between the pMC/PCL phase and the cMC/PCL phase, where no distinct boundary is observed, and the pore size gradually decreases until it disappears in the cMC/PCL phase.

PCL phase. Fig. 3C, D, and 3E display cross-sectional images in different orientations, clearly revealing the internal porous structure and dense regions of the scaffold.

Fig. 3F, G, and 3H show the microstructures of the pMC/PCL, cMC/PCL, and bMC/PCL scaffolds observed by SEM. The pMC/PCL scaffold exhibited a typical interconnected and hierarchical porous structure, while the cMC/PCL scaffold showed a compact morphology. In the bMC/PCL scaffold, there was no distinct boundary separating the pMC/PCL phase from the cMC/PCL phase; instead, an interfacial bonding zone appeared, where the pore size gradually decreased until disappearing in the cMC/PCL phase. This interfacial bonding zone highly mimics the natural interface structure between cancellous and cortical bone, facilitating the tight connection between the pMC/PCL and cMC/PCL phases and contributing to the overall integrity of the bMC/PCL scaffold.

Mechanical tests were conducted to measure the compressive strength and elastic modulus of the pMC/PCL, cMC/PCL, and bMC/PCL scaffolds. As shown in Table 1, the compressive strength and elastic modulus of the cMC/PCL scaffold (31.26 ± 1.31 MPa, 2.15 ± 0.20 GPa) were significantly higher than those of the pMC/PCL scaffold (0.86 ± 0.01 MPa, 0.05 ± 0.01 GPa). The bMC/PCL scaffold exhibited compressive strength and elastic modulus values (20.73 ± 0.43 MPa, 1.68 ± 0.27 GPa) that fell between those of the pMC/PCL and cMC/PCL scaffolds. These differences are mainly attributed to the varying microstructures of the scaffolds, particularly the dense microstructure of the cMC/PCL scaffold.

Since the pMC/PCL and bMC/PCL scaffolds share the same composition, their significantly different mechanical properties are primarily due to the presence of the cMC/PCL phase in the bMC/PCL scaffold. In comparison, the compressive strength of cancellous bone ranges from 1 to 10 MPa, and its elastic modulus ranges from 0.10 to 3 GPa. The compressive strength of cortical bone ranges from 100 to 200 MPa, and its elastic modulus ranges from 10 to 20 GPa. The mechanical properties of the cMC/PCL scaffold most closely resemble those of cortical bone, while the pMC/PCL and bMC/PCL scaffolds exhibit mechanical properties that lie between those of cancellous and cortical bone. Specifically, the cMC/PCL scaffold demonstrates a significant advantage in compressive strength and elastic modulus, indicating its potential for bearing higher mechanical loads.

In this study, the pMC/PCL scaffolds exhibited a porosity of 73.20 ± 1.70 %, providing favorable conditions for cell infiltration and nutrient transport, thereby promoting bone tissue regeneration. In contrast, the bMC/PCL composite scaffolds had a porosity of 41.86 ± 1.77 %, indicating a lower porosity. This is primarily due to the cMC/PCL component, which serves as the main structural support of the scaffold. To ensure high mechanical performance, the cMC/PCL scaffolds were designed with a low porosity of approximately 1–5 %. Overall, the bMC/PCL scaffolds integrate the high-porosity pMC/PCL in the outer region with the low-porosity cMC/PCL in the inner region, meeting the requirements for osteogenesis while enhancing mechanical properties, making them suitable for applications demanding high mechanical performance.

The biocompatibility of the materials involved in this paper has been repeatedly verified in previous studies by our team, demonstrating their good adaptability and promoting effect on bone marrow stem cells [26, 31,32]. The results from co-culture fluorescent staining, Alizarin Red staining, and CCK-8 experiments indicate that pMC/PCL materials exhibit advantages in promoting bone marrow stem cell attachment, spreading, and proliferation. The corresponding data have been included in the supplementary materials (Fig. S1).

**Table 1**
Mechanical properties of materials.

| | pMC/PCL | cMC/PCL | bMC/PCL | cancellous bone | compact bone |
|---|---|---|---|---|---|
| compressive strength (MPa) | 0.86 ± 0.01 | 31.26 ± 1.31 | 20.73 ± 0.43 | 1–10 | 100–200 |
| elasticity modulus (GPa) | 0.05 ± 0.01 | 2.15 ± 0.20 | 1.68 ± 0.27 | 0.10–3 | 10–20 |

### 3.2. X-ray evaluation of bone repair

The occurrence of bone plate fractures in the blank group was particularly severe during the experimental period, with all bone plates experiencing breakage. At the 3-month postoperative X-ray examination, all 10 sheep in the blank group showed fixation failure, with 4 out of 10 experiencing bone plate fractures and 6 out of 10 experiencing screw fractures. These data reveal significant deficiencies in the bone plate's performance during the repair process in the blank group. In contrast, the experimental group demonstrated markedly better outcomes. In the experimental group, only 1 out of 10 sheep experienced screw fractures at the 3-month postoperative X-ray examination.

Fig. 4 illustrates the X-ray results of the blank and experimental groups at different postoperative time points (3 months and 6 months), showing the instances of bone plate and screw fractures as well as the bone defect repair status. The X-ray images of the blank group at immediate postoperative and 3 months (Fig. 4A) indicate that all bone plates and screws had fractured by 3 months, leading to fixation failure. Conversely, the X-ray images of the experimental group at immediate postoperative and 3 months (Fig. 4B) show stable fixation at the bone defect site, with significant callus formation observed at 3 months. Further X-ray images (Fig. 4C) demonstrate that the bone defect site in the experimental group remained stably fixed at immediate postoperative, 3 months, and 6 months, with the bone defect being completely repaired by 6 months.

The Lane-Sandhu scoring system was used to evaluate the bone repair status with the bMC/PCL scaffolds (Fig. 5C). The results showed that the Lane-Sandhu scores in the blank group remained at 1, mainly due to the complete fracture of the bone plates and screws, resulting in no healing at the bone defect site. In the experimental group, the Lane-Sandhu score was 3.60 ± 0.548 at 3 months and 4.00 ± 0.707 at 6 months, with a significant difference ($t = 3.500$, $p = 0.008$). Compared to the blank group, the experimental group demonstrated higher healing scores at both 3 and 6 months, indicating that the bMC/PCL scaffold material effectively promoted callus formation and bone bridging in the early stages, with the repair effect further enhanced over time (see Fig. 6).

### 3.3. Lameness evaluation

In this study, the VAS was used to evaluate the lameness of sheep (as shown in Fig. 5B). Statistical analysis of lameness scores at different time points was performed to assess the differences between the blank group and the bMC/PCL scaffold group. At 1 month post-surgery, the average lameness score for the blank group was 8.11 ± 1.52, and for the bMC/PCL scaffold group, it was 6.76 ± 1.22, with no significant difference ($q = 2.496$, $p = 0.497$). At 3 months post-surgery, the blank group's score decreased to 6.59 ± 2.42, while the bMC/PCL scaffold group's score decreased to 2.71 ± 0.97, showing a significant difference ($q = 7.173$, $p < 0.0001$). At 6 months post-surgery, the blank group's score was 6.00 ± 2.23, whereas the bMC/PCL scaffold group's score further decreased to 1.48 ± 0.86, with a significant difference ($q = 6.823$, $p = 0.0002$). The results indicate that the bMC/PCL scaffold significantly reduced the lameness scores at 3 and 6 months post-surgery, demonstrating its effectiveness in promoting bone defect repair and improving functional recovery. Although the difference between the groups was not significant at 1 month post-surgery, this might be due to the early stage of repair when the advantages of the bMC/PCL scaffold had not yet fully manifested. However, as time progressed, the advantages of the bMC/PCL scaffold in promoting callus formation and bone bridging became apparent, ultimately showing significant repair effects at 3 and 6 months post-surgery.

### 3.4. Micro-CT image analysis

Micro-CT technology was employed to evaluate bone repair at 3 and 6 months post-surgery. Fig. 5A presents the Micro-CT images of large segmental bone defect repair at 3 months and 6 months post-surgery. The top row shows three-dimensional reconstruction images, with the red box area indicating the bone defect site. The bottom row shows the corresponding two-dimensional cross-sectional images. At 3 months post-surgery, the defect area exhibited partial bone regeneration, but bone bridging was not yet complete. At 6 months post-surgery, the defect area showed significantly increased bone regeneration, more complete bone bridging, and complete repair of the bone defect, demonstrating significant bone repair effects. At 6 months post-surgery, the tight integration of new bone with the scaffold material was clearly visible. Additionally, the scaffold material had undergone significant degradation. The bMC/PCL scaffold not only promoted new bone formation but also gradually degraded over time, leaving space for the further growth of new bone tissue.

Quantitative analysis of the Micro-CT images revealed significant increases in BV/TV and BMD, along with a significant increase in Tb.Th and a significant decrease in Tb.Sp at 6 months post-surgery. Specifically, the BV/TV increased from 28.07 ± 9.22 % at 3 months post-surgery to 62.02 ± 11.82 % at 6 months post-surgery, with a significant difference ($t = 5.064$, $p = 0.001$) (Fig. 5D). The BMD increased from 0.392 ± 0.032 g/cm$^3$ at 3 months post-surgery to 0.583 ± 0.125 g/cm$^3$ at 6 months post-surgery, with a significant difference ($t = 3.327$, $p = 0.0104$) (Fig. 5E). The Tb.Th increased from 0.690 ± 0.224 mm at 3 months post-surgery to 1.049 ± 0.089 mm at 6 months post-surgery, with a significant difference ($t = 3.333$, $p = 0.0103$) (Fig. 5F). The Tb.Sp decreased from 2.766 ± 1.183 mm at 3 months post-surgery to 0.501 ± 0.268 mm at 6 months post-surgery, with a significant difference ($t = 4.175$, $p = 0.0031$) (Fig. 5G). These results indicate that the bMC/PCL scaffold shows excellent performance in large segmental bone defect repair, effectively promoting bone tissue regeneration, increasing bone density, and improving bone structure. All control groups (i.e., the blank

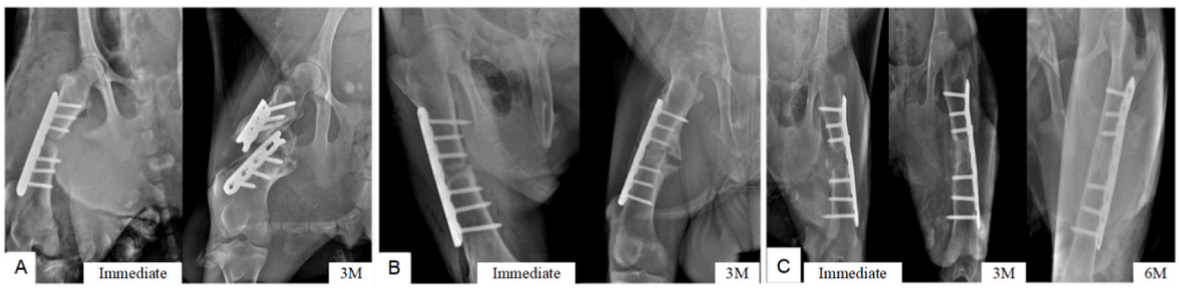


**Fig. 4.** X-ray results of the control and experimental groups at different time points (3M and 6M) post-operation, demonstrating the incidence of plate and screw breakage and the repair of bone defects. (A) X-ray images of the control group immediately post-operation and at 3 months, showing plate/screw breakage and fixation failure at 3 months post-operation. (B) X-ray images of the experimental group immediately post-operation and at 3 months, showing stable fixation at the bone defect site and callus formation at 3 months post-operation. (C) X-ray images of the experimental group immediately post-operation, at 3 months, and at 6 months, showing stable fixation at the bone defect site and complete repair of the bone defect at 6 months post-operation.

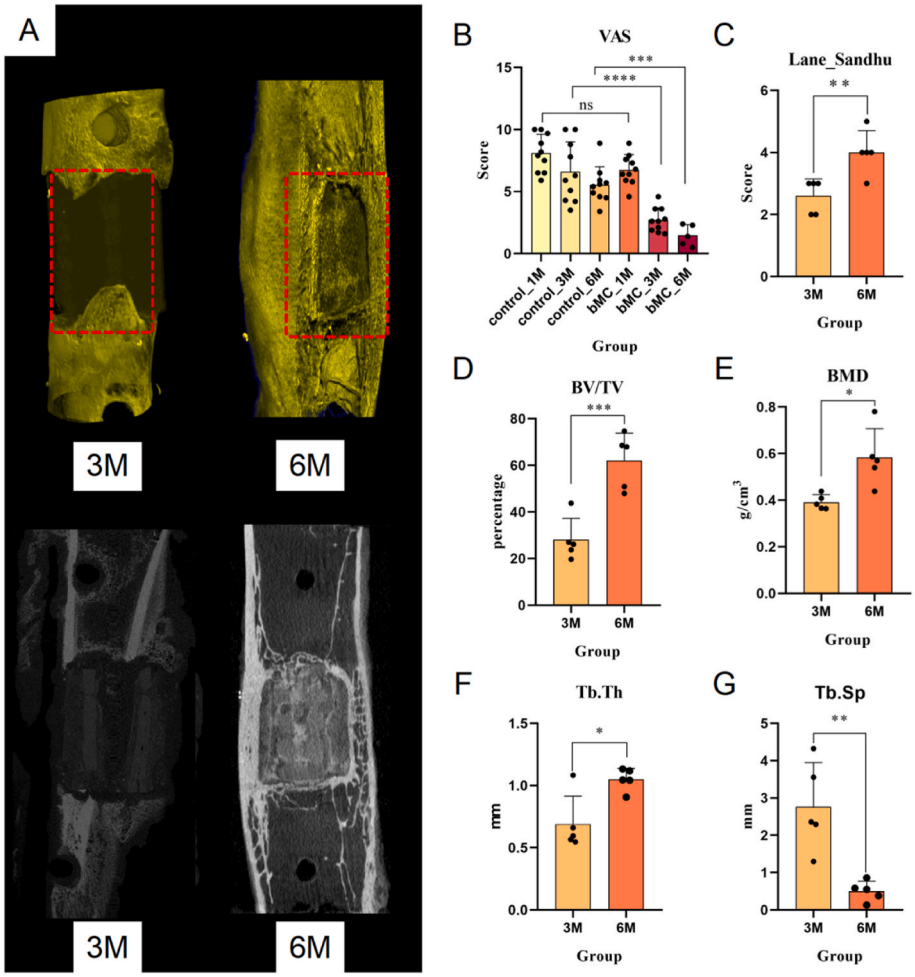


**Fig. 5.** Bone defect repair in Small Tail Han sheep in the control and experimental groups at different time points. (A) Micro-CT images showing the 3D reconstructed images and 2D cross-sectional images of the bone defect area at 3 months and 6 months post-operation, with the bone defect area highlighted in red boxes. (B) VAS scores displaying the changes in limping scores of the control and experimental groups at 1 month, 3 months, and 6 months post-operation, with the experimental group showing significantly lower limping scores compared to the control group (****$p < 0.0001$). (C) Lane-Sandhu scores displaying the bone repair scores of the experimental group at 3 months and 6 months post-operation, with the scores at 6 months being significantly higher than those at 3 months (**$p < 0.01$). (D) Changes in BV/TV at 3 months and 6 months post-operation, with the volume at 6 months being significantly higher than at 3 months (***$p < 0.001$). (E) Changes in BMD at 3 months and 6 months post-operation, with the density at 6 months being significantly higher than at 3 months (*$p < 0.05$). (F) Changes in Tb.Th at 3 months and 6 months post-operation, with the thickness at 6 months being significantly higher than at 3 months (*$p < 0.05$). (G) Changes in Tb.Sp at 3 months and 6 months post-operation, with the spacing at 6 months being significantly lower than at 3 months (**$p < 0.01$).

groups without implanted materials) exhibited plate fractures with no healing observed. Therefore, based on the experimental design and observational results, we did not perform μ-CT imaging analysis on the control groups, as no valid healing data were generated for evaluation.

### 3.5. Histological evaluation of regenerated bone

At 3 months and 6 months post-surgery, HE staining and Masson staining of bone tissue sections were used to show the progress of bone regeneration. At 3 months post-surgery, HE staining results showed new bone formation at the ends of the bone defect, with cell infiltration observed within the scaffold material. However, there were still significant gaps in the bone defect area, with minimal callus formation and limited bone regeneration, and no bony bridging was observed between the defect ends. At 6 months post-surgery, there was a significant increase in callus formation in the bone defect area, with most of the defect filled with newly formed bone tissue. Bony bridging had been established, and the new bone trabecular structure was more mature and dense, with cortical bone thickness approaching that of normal cortical bone, indicating substantial enhancement in bone regeneration. Masson staining further corroborated these findings. At 3 months post-surgery, the defect area was primarily filled with fibrous tissue, with minimal new bone tissue and sparse trabecular structure, indicating insufficient bone regeneration. By 6 months post-surgery, the defect area was filled with a significant amount of new bone tissue, with clearly visible trabecular structures. The new bone tissue was tightly integrated with the original bone tissue, showing a dense trabecular structure. At this stage, the scaffold material had significantly degraded, and new bone growth was observed within the space left by the degrading material. These results indicate that over time, the bMC/PCL scaffold significantly promotes bone regeneration and repair. The substantial new bone formation and integration with existing bone tissue observed at 6 months post-surgery demonstrate the scaffold's efficacy in enhancing bone healing and structural integrity. The scaffold's ability to degrade and create space for new bone growth further supports its role in effective bone repair. A statistical evaluation was conducted on the area ratio between the material and newly formed bone in the tissue sections. The results (see Supplementary Fig. S2) showed that at 3 months post-operatively, the material area/bone area ratio in the experimental group was 145.28 % ± 0.215. By 6 months postoperatively, this ratio had

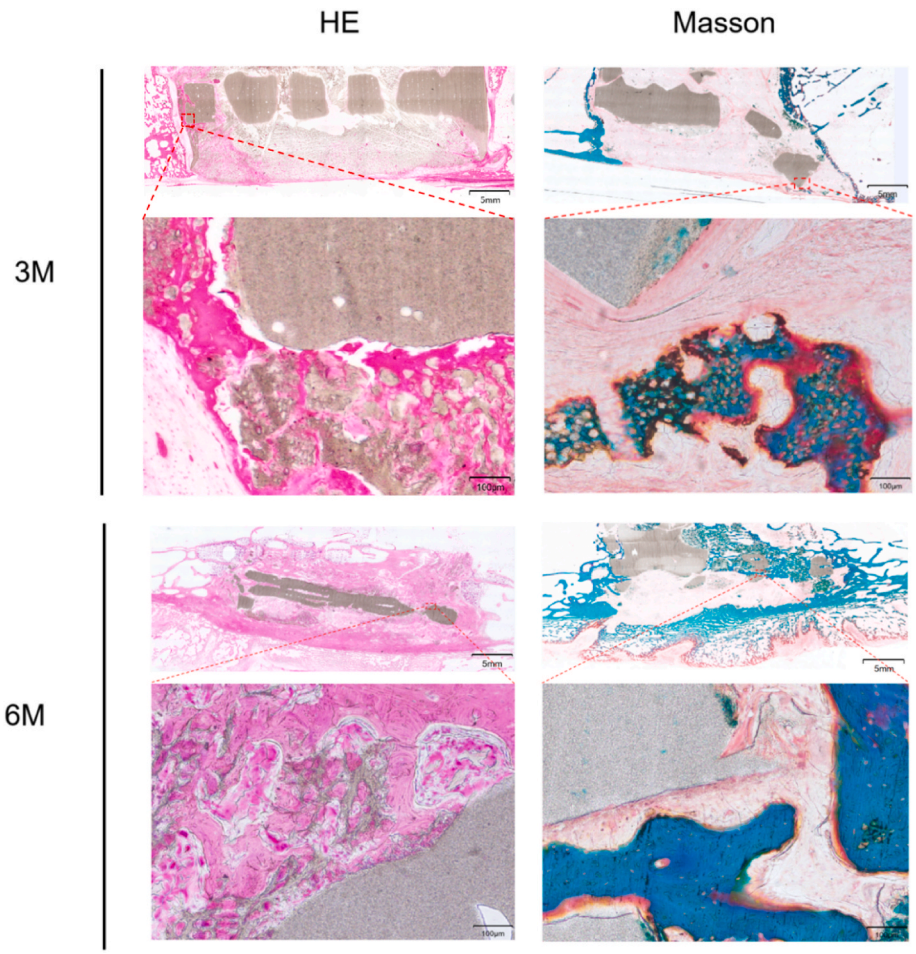


**Fig. 6.** HE and Masson staining results at 3 months and 6 months post-operation. At 3 months post-operation, new bone formation is visible at the ends of the bone defect, and cellular infiltration is observed within the material, but no bony connection has formed between the ends. At 6 months post-operation, bony connections have formed, and the cortical bone thickness is close to that of normal cortex, indicating successful repair of the bone defect. Additionally, the material has significantly degraded, and new bone growth can be seen in the spaces left by the degraded material.

decreased to 44.97 % ± 0.056. These findings indicate that as the implantation time increases, the scaffold is gradually replaced by newly formed bone tissue in the mid-to-late stages, leading to a continuous improvement in the bone repair process. This confirms the excellent osteoinductive and tissue integration capabilities of the composite scaffold.

### 3.6. Nanoindentation experiment

As shown in Fig. 7, to further evaluate the mechanical properties of neogenic bone during the bone repair process, this study conducted nanoindentation tests to compare the hardness and Young's modulus of neogenic bone at 3 months and 6 months with those of natural bone. The results indicate that at 3 months, the hardness of neogenic bone was 0.47 ± 0.12 GPa, approximately 53 % of that of natural bone (0.88 ± 0.16 GPa) ($p < 0.001$) (Fig. 7A). The Young's modulus of neogenic bone was 11.72 ± 1.69 GPa, about 63 % of that of natural bone (18.48 ± 1.64 GPa) ($p < 0.0001$) (Fig. 7C). By 6 months, the hardness of neogenic bone had increased to 0.59 ± 0.05 GPa, roughly 69 % of that of natural bone (0.85 ± 0.17 GPa) ($p < 0.01$) (Fig. 7B), while its Young's modulus increased to 14.93 ± 1.47 GPa, about 80 % of that of natural bone (18.74 ± 1.82 GPa) ($p < 0.01$) (Fig. 7D). Overall, from 3 to 6 months, the neogenic bone showed a significant increase in both hardness and Young's modulus, gradually approaching the values observed for natural bone.

## 4. Discussion

In bone tissue engineering, finding materials that can mimic the structure and function of natural bone tissue is a critical research direction. The application of PCL in bone tissue engineering has garnered widespread attention, especially as a biomaterial for treating bone defects [33–37]. Its unique biodegradability, excellent biocompatibility, and favorable mechanical properties make it an ideal biomedical material. Studies have shown that composite scaffolds combining PCL with natural materials can effectively promote bone reconstruction and provide a suitable microenvironment for the proliferation and osteogenic differentiation of human bone-derived cells [38]. In recent years, MC/PCL scaffolds have emerged as a promising choice due to their excellent biocompatibility and mechanical properties [39–43]. Various studies have demonstrated that MC/PCL scaffolds exhibit superior performance in supporting cell attachment, proliferation, migration, and osteogenic differentiation [39,40]. While MC/PCL scaffolds have achieved some success in bone repair models [39,41], their effectiveness in repairing large bone defects still requires improvement [42]. Although the incorporation of PCL can enhance the mechanical strength of mineralized collagen scaffolds, the mechanical properties of these scaffolds still fall short of the requirements for use in load-bearing sites. Improving the mechanical performance of these scaffolds to meet both the demands of bioactivity and the physiological load-bearing requirements remains a challenge that needs further research. Ensuring that the scaffold can support the physical demands of load-bearing while

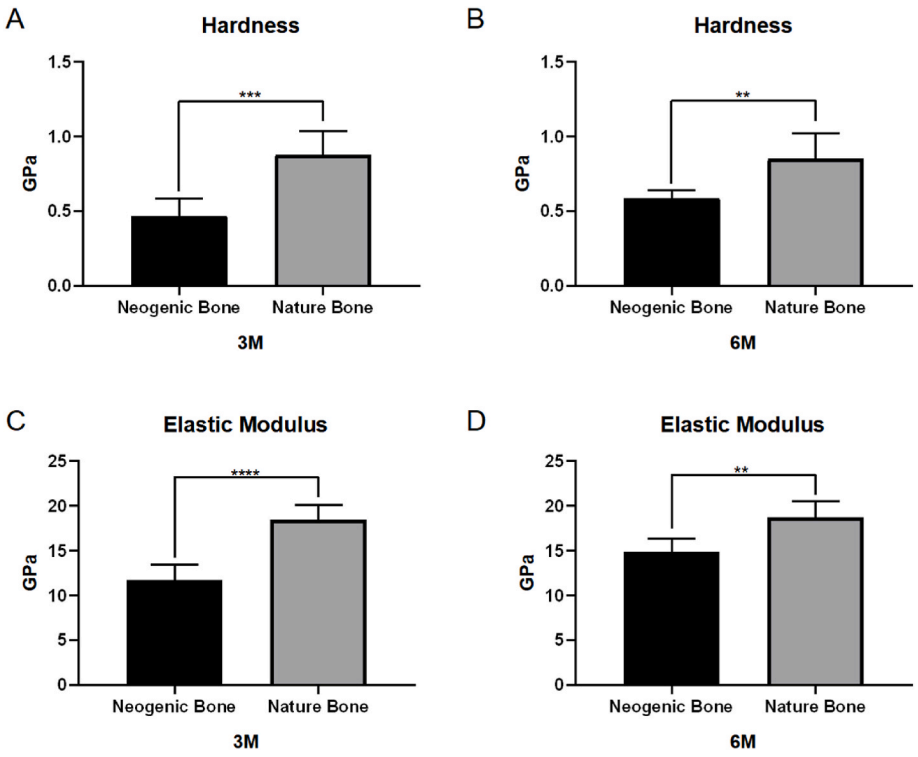


**Fig. 7.** Results of the nanoindentation experiment measuring the hardness and Young's modulus of neogenic bone (Neogenic Bone) and natural bone (Nature Bone) at 3 months (3M) and 6 months (6M). (A) and (C) At 3 months, the hardness and Young's modulus of neogenic bone are about 53 % and 63 % of those of natural bone, respectively. (B) and (D) At 6 months, these values increase to approximately 69 % and 80 % of those of natural bone, respectively. *$p < 0.05$, **$p < 0.01$, and ***$p < 0.001$ denote statistically significant differences.

also promoting bone regeneration is essential for advancing the application of MC/PCL scaffolds in clinical settings.

The bMC/PCL scaffold used in this study integrates the porous characteristics of the pMC/PCL scaffold with the high mechanical stability of the cMC/PCL scaffold, forming a "bilayer composite" scaffold with a hierarchical internal and external structure. The outer layer, composed of pMC/PCL, features a rich porous structure that facilitates cell adhesion, vascularization, and bone tissue ingrowth into the scaffold. Meanwhile, the cMC/PCL core provides enhanced mechanical strength, effectively supporting the mechanical stress required for load-bearing bone healing. Compared to standalone pMC/PCL or cMC/PCL scaffolds, the bMC/PCL scaffold combines the advantages of both, addressing the need for both bioactivity and load-bearing capacity in large bone defect repair. This study highlights the potential of bMC/PCL scaffolds in treating large load-bearing bone defects, laying a foundation for further optimization of scaffold design to balance mechanical strength and biological functionality.

In our previous study [19], we addressed the trade-off between mechanical support and osteogenic capacity in MC/PCL scaffolds. We developed the bMC/PCL scaffold, which combines the osteogenic advantages of the pMC/PCL scaffold with the mechanical integrity advantages of the cMC/PCL scaffold. In an in vivo study conducted on one-month-old sheep, promising results were observed: the pMC/PCL scaffold promoted increased bone density and complete bone bridge connection, while the cMC/PCL framework provided mechanical protection without significant degradation. However, this animal experiment was conducted in non-load-bearing sites. To broaden the application scenarios of the bMC/PCL scaffold, in this study, we optimized the structure design of the cMC/PCL scaffold based on the structural characteristics of the repair site (femur), and then embedded it into the pMC/PCL matrix. We comprehensively evaluated the application potential of the bMC/PCL scaffold in large load-bearing bone defects such as the femur. This is significantly different from previous studies that mainly focused on non-load-bearing bones or small bone defects. Additionally, we chose Small Tail Han sheep as the experimental animals, whose bone quality and bone mass are more comparable to humans, which helps to improve the clinical relevance of the research results [44].

From both the perspectives of load-bearing capacity and bioactivity, the bMC/PCL scaffold demonstrates ideal characteristics. Mechanical testing and animal experiment results show that bMC/PCL has advantages in effectively supporting bone plates and screws, as well as significantly reducing the fracture rate of the fixator. This supports the idea that the scaffold provides sufficient mechanical stability for large-load bone repair. Meanwhile, bMC/PCL significantly promotes new bone formation, outperforming the control group in terms of bone defect repair scores, lameness scores, Micro-CT evaluation, and histological staining, with further improvements over time. This suggests that by embedding pMC/PCL into cMC/PCL, we not only enhance the scaffold's mechanical compatibility in load-bearing environments but also take advantage of the cellular adhesion and osteogenic benefits provided by the highly porous material. Histological results show that at 3 months postoperatively, the material area to newly formed bone area ratio in the experimental group was approximately 145.28 % ± 0.215. At 6 months postoperatively, this ratio decreased to 44.97 % ± 0.056. The significant reduction in this ratio clearly indicates that, with the passage of time, the scaffold is gradually replaced by bone tissue in the body, with newly formed bone continuously filling the defect area. This process of bone replacement is also visually reflected in the histological images of this experiment, demonstrating the scaffold's ideal "weight-bearing first, degradation later" effect.

Additionally, our results demonstrated that the bMC/PCL scaffolds significantly promote new bone formation. Bone repair scores, limping scores, Micro-CT evaluations, and histomorphological experiments all indicated that the bMC/PCL scaffolds were more effective in repairing femoral bone defects compared to the control group, with significant

improvements observed over time. This result confirms another goal of our design, which was to enhance the bioactivity of the cMC/PCL scaffold by embedding pMC/PCL within the cMC/PCL framework.

Our findings are also complemented by other studies. Their research demonstrated that integrating a PCL reinforcing structure with a mineralized collagen-glycosaminoglycan composite biomaterial can overcome the traditional trade-off between mechanical strength and bioactivity [40,45]. Their results showed that the PCL support framework determined most of the mechanical response of the composite, with the modulus increasing by 6000 times compared to the mineralized scaffold alone. Similarly, as a composite of the pMC/PCL scaffold and the cMC/PCL scaffold, the bMC/PCL scaffold retains the bioactivity of the pMC/PCL scaffold while also possessing the strength of the cMC/PCL scaffold. Another study demonstrated that MC has a comparable effect to autologous bone in remodeling femoral defects [46].

In previous studies, scaffold performance in large segmental weight-bearing bone defect models has been systematically evaluated, providing valuable points of comparison for our work. For instance, Crovace et al. [47] applied EBM-sintered titanium alloy scaffolds in a 5 cm tibial defect, facilitating immediate postoperative weight-bearing and restoring normal gait by 2 months. In contrast, animals treated with porous hydroxyapatite scaffolds experienced internal fixation failure within 1 month due to excessive loading. Although our study involved a shorter 2 cm defect and a different fixation approach, only one sheep in the bMC/PCL scaffold group exhibited screw breakage at 3 months postoperatively, whereas the blank group demonstrated widespread plate or screw fractures during the same period. These findings suggest that the bMC/PCL scaffold not only provides the mechanical stability required for large-segment bone defect repair but also supports continued bone regeneration from 3 to 6 months. Additionally, in a 2.5 cm metatarsal mid-shaft defect model with external fixation, Garot et al. [48] observed complete or partial defect bridging in most animals by 4 months, although their scaffold was combined with the exogenous growth factor BMP-2. In our study, even without exogenous proteins or stem cells, the bMC/PCL scaffold achieved partial bridging at 3 months and complete defect repair at 6 months, indicating an osteogenic capacity comparable to that of scaffolds relying on exogenous factors. Similarly, Cipitria et al. [49], using a BMP-7-loaded PCL/tricalcium phosphate scaffold for a 3 cm sheep tibial defect, found complete bridging as early as 3 months, and by 12 months the mechanical properties of the newly formed bone approached those of native bone. In our experiment, the hardness and Young's modulus of the regenerated bone increased progressively, reaching approximately 69 % and 80 %, respectively, of normal bone values at 6 months. Likewise, Liu et al. [50] investigated a 2.5 cm sheep tibial defect using a nano-hydroxyapatite/collagen/polylactic acid/chitin fiber scaffold seeded with bone marrow stem cells, demonstrating nearly 99 % of normal tibial bending strength by 8 weeks—though that approach incorporated seeded cells. By contrast, our bMC/PCL scaffold, even without exogenous growth factors or stem cells, maintained robust mechanical stability, reduced the incidence of internal fixation failure, and achieved satisfactory new bone bridging and fusion within 6 months. By integrating a dense inner layer for load-bearing capacity with a highly porous outer layer for cell adhesion and nutrient transport, the bMC/PCL composite scaffold appears to offer a promising solution that balances mechanical support and bone regeneration for the repair of large segmental bone defects.The comprehensive advantages of the bMC/PCL scaffold are particularly noteworthy. This scaffold not only combines the bioactivity of the pMC/PCL scaffold with the mechanical strength of the cMC/PCL scaffold but also, through meticulous structural design and optimization, has the potential to achieve more complex and refined bone defect repairs. This innovative approach may provide more options and greater flexibility for bone defect repair, especially when dealing with load-bearing bone defects that require prolonged and high-strength support. Therefore, the integrated performance of the bMC/PCL scaffold holds great promise for future clinical applications. Overall, this study offers a new possibility for the repair of large load-bearing bone defects.

However, despite the positive significance of our findings, there are some issues that need attention. Firstly, while our results indicate that the bMC/PCL scaffold is effective in repairing large load-bearing bone defects, these results are based on the Small Tail Han sheep model, which has limited similarity to humans. Therefore, our results need to be validated in a broader range of animal models and ultimately confirmed in human clinical trials. Secondly, our study did not thoroughly investigate the biodegradation process and mechanisms of the bMC/PCL scaffold, which is an area that requires further in-depth research. Thirdly, while we used the VAS scale to assess lameness, which is a commonly used subjective measure in clinical settings, we acknowledge that gait analysis could provide more objective and comprehensive insights into walking ability. However, gait analysis was not included in the scope of this study, which limits the thorough evaluation of lameness and walking function. Finally, our study focused solely on the repair efficacy of the composite scaffold and did not consider potential side effects, such as possible inflammatory responses and hypersensitivity reactions, which also need to be explored in future research.

## 5. Conclusion

This study evaluated the effectiveness of the bMC/PCL scaffold in repairing large load-bearing bone defects, demonstrating significant advantages in promoting bone defect healing. The research indicates that the bMC/PCL scaffold combines the bioactivity of the pMC/PCL scaffold with the mechanical strength of the cMC/PCL scaffold, optimizing the scaffold's mechanical performance and structural characteristics. In terms of functional recovery, the experimental group showed significant improvements compared to the control group. Furthermore, X-ray, Micro-CT, and histological analyses revealed that the bMC/PCL scaffold significantly promoted new bone formation, effectively encouraging new bone growth while gradually degrading, thus providing a conducive environment for new bone tissue development. Over time, there was a notable increase in bone volume and bone density, with trabecular thickness increasing and trabecular spacing decreasing. Consequently, the bMC/PCL scaffold exhibited excellent bioactivity and mechanical performance in repairing large load-bearing bone defects, indicating promising clinical application prospects. Future research should further validate the safety and efficacy of this scaffold in a broader range of animal models to support its clinical application.

## Consent to participate

Informed consent was obtained from all participants involved in the study.

## Consent to publish

All authors and contributors have agreed to publish the findings of this study.

## Ethical approval

This study was approved by the Institutional Animal Care and Use Committee (IACUC) of Tsinghua University, under the IACUC Identification Number 22-WXM4. The study was conducted in compliance with the guidelines and regulations set forth by the IACUC. Ethical approval for human participant involvement was not required as the study did not involve human subjects.

## Authors contributions

Meng-Xuan Yao contributed to the conceptualization, methodology, large animal experiments, and writing of the original draft. Jing-Chuan

Zheng was responsible for the preparation of bioactive materials used in the experiments. Hai-Cheng Wang also contributed to the large animal experiments. Hong-Zhi Lv, Yi-Fan Zhang, Yu-Qin Zhang, Tai-Long Shi, and Yan-Ze Zhu were involved in data curation. Ying-Ze Zhang provided supervision. Xiu-Mei Wang and Wei Chen contributed to the conceptualization, supervision, project administration, and writing – review & editing.

## Funding

We acknowledge the financial support from the National Key R&D Program of China (2020YFC1107601), the National Natural Science Youth Foundation of China (Grant No. 82102584), and the 2024 Hebei Province Doctoral Student Innovation Ability Training Project (CXZZBS2024124).

## Conflict of interest statement

The authors declare that there is no conflict of interest regarding the publication of this paper.

## Appendix A. Supplementary data

Supplementary data to this article can be found online at https://doi.org/10.1016/j.jot.2025.03.014.

## References

[1] Sun Y, Wang C-Y, Wang Z-Y, Cui Y, Qiu Z-Y, Song T-X, et al. Test in canine extraction site preservations by using mineralized collagen plug with or without membrane. J Biomater Appl 2016;30:1285–99.
[2] Xuan Y, Li L, Ma M, Cao J, Zhang Z. Hierarchical intrafibrillarly mineralized collagen membrane promotes guided bone regeneration and regulates M2 macrophage polarization. Front Bioeng Biotechnol 2022;9:781268.
[3] Zhu W, Li C, Yao M, Wang X, Wang J, Zhang W, et al. Advances in osseointegration of biomimetic mineralized collagen and inorganic metal elements of natural bone for bone repair. Regen Biomater 2023:rbad030.
[4] Diogo GS, Marques CF, Freitas-Ribeiro S, Sotelo CG, Pérez-Martin RI, Pirraco RP, et al. Mineralized collagen as a bioactive ink to support encapsulation of human adipose stem cells: a step towards the future of bone regeneration. Biomater Adv 2022;133:112600.
[5] Dewey MJ, Johnson EM, Weisgerber DW, Wheeler MB, Harley BAC. Shape-fitting collagen-PLA composite promotes osteogenic differentiation of porcine adipose stem cells. J Mech Behav Biomed Mater 2019;95:21–33.
[6] Sarmiento M, Ramírez P, Parody R, Salas MQ, Beffermann N, Jara V, et al. Advantages of non-cryopreserved autologous hematopoietic stem cell transplantation against a cryopreserved strategy. Bone Marrow Transplant 2018;53:960–6.
[7] Windhager R, Hobusch GM, Matzner M. Allogeneic transplants for biological reconstruction of bone defects. Orthopä 2017;46:656–64.
[8] Wang Y-H, Zhao C-Z, Wang R-Y, Du Q-X, Liu J-Y, Pan J. The crosstalk between macrophages and bone marrow mesenchymal stem cells in bone healing. Stem Cell Res Ther 2022;13:511.
[9] Zhu Q, Jiao H, Zhao X, Tang Y, Zhao K, Gou X. Hydroxyapatite formation in biomimetic synthesis with the interface of a pDA@ SIS membrane. RSC Adv 2022;12:13209–19.
[10] Fu Y, Liu S, Cui S-J, Kou X-X, Wang X-D, Liu X-M, et al. Surface chemistry of nanoscale mineralized collagen regulates periodontal ligament stem cell fate. ACS Appl Mater Interfaces 2016;8:15958–66.
[11] de Melo Pereira D, Habibovic P. Biomineralization-inspired material design for bone regeneration. Adv Healthcare Mater 2018;7:1800700.
[12] Marelli B, Ghezzi CE, James-Bhasin M, Nazhat SN. Fabrication of injectable, cellular, anisotropic collagen tissue equivalents with modular fibrillar densities. Biomaterials 2015;37:183–93.
[13] Brown M, Li J, Moraes C, Tabrizian M, Li-Jessen NYK. Decellularized extracellular matrix: new promising and challenging biomaterials for regenerative medicine. Biomaterials 2022:121786.
[14] Xing H, Lee H, Luo L, Kyriakides TR. Extracellular matrix-derived biomaterials in engineering cell function. Biotechnol Adv 2020;42:107421.
[15] Jin S-S, He D-Q, Luo D, Wang Y, Yu M, Guan B, et al. A biomimetic hierarchical nanointerface orchestrates macrophage polarization and mesenchymal stem cell recruitment to promote endogenous bone regeneration. ACS Nano 2019;13:6581–95.
[16] Yu L, Rowe DW, Perera IP, Zhang J, Suib SL, Xin X, et al. Intrafibrillar mineralized collagen–hydroxyapatite-based scaffolds for bone regeneration. ACS Appl Mater Interfaces 2020;12:18235–49.
[17] Li J, Zhang Y-J, Lv Z-Y, Liu K, Meng C-X, Zou B, et al. The observed difference of macrophage phenotype on different surface roughness of mineralized collagen. Regen Biomater 2020;7:203–11.
[18] Bharadwaz A, Jayasuriya AC. Recent trends in the application of widely used natural and synthetic polymer nanocomposites in bone tissue regeneration. Mater Sci Eng C 2020;110:110698.
[19] Zheng J, Zhao Z, Yang Y, Wang S, Zhao Y, Xiong Y, et al. Biphasic mineralized collagen-based composite scaffold for cranial bone regeneration in developing sheep. Regen Biomater 2022;9:rbac004.
[20] Frost HM. Wolff's Law and bone's structural adaptations to mechanical usage: an overview for clinicians. Angle Orthod 1994;64:175–88.
[21] Perin M, Chinigò G, Genova T, Mussano F, Munaron L. The impact of plasma membrane ion channels on bone remodeling in response to mechanical stress, oxidative imbalance, and acidosis. Antioxidants 2023;12:689.
[22] Wu X, Gauntlett O, Zhang T, Suvarnapathaki S, McCarthy C, Wu B, et al. Eggshell microparticle reinforced scaffolds for regeneration of critical sized cranial defects. ACS Appl Mater Interfaces 2021;13:60921–32.
[23] Tong L, Pu X, Liu Q, Li X, Chen M, Wang P, et al. Nanostructured 3D-printed hybrid scaffold accelerates bone regeneration by photointegrating nanohydroxyapatite. Adv Sci 2023;10:2300038.
[24] Zhong Z, Wu X, Wang Y, Li M, Li Y, Liu X, et al. Zn/Sr dual ions-collagen co-assembly hydroxyapatite enhances bone regeneration through procedural osteo-immunomodulation and osteogenesis. Bioact Mater 2022;10:195–206.
[25] Cui F-Z, Li Y, Ge J. Self-assembly of mineralized collagen composites. Mater Sci Eng R Rep 2007;57:1–27.
[26] Wang S, Yang Y, Zhao Z, Wang X, Mikos AG, Qiu Z, et al. Mineralized collagen-based composite bone materials for cranial bone regeneration in developing sheep. ACS Biomater Sci Eng 2017;3:1092–9.
[27] Wang S, Yang Y, Koons GL, Mikos AG, Qiu Z, Song T, et al. Tuning pore features of mineralized collagen/PCL scaffolds for cranial bone regeneration in a rat model. Mater Sci Eng C 2020;106:110186.
[28] Wang S, Zhao Z, Yang Y, Mikos AG, Qiu Z, Song T, et al. A high-strength mineralized collagen bone scaffold for large-sized cranial bone defect repair in sheep. Regen Biomater 2018.
[29] Gao C, Gao J, Tian W, Hou J, Wang X, Jia X, et al. Clinical observation on repair of limbs bone defect by using mineralized collagen graft. Chinese Journal of Primary Medicine and Pharmacy 2017:1775–8.
[30] Welsh EM, Gettinby G, Nolan AM. Comparison of a visual analogue scale and a numerical rating scale for assessment of lameness, using sheep as a model. American journal of veterinary research 1993;54:976–83.
[31] Wang S, Zhao Z, Yang Y, Mikos AG, Qiu Z, Song T, et al. A high-strength mineralized collagen bone scaffold for large-sized cranial bone defect repair in sheep. Regen Biomater 2018;5:283–92.
[32] He Y, Wang Q, Liu Y, Zhang Z, Cao Z, Wang S, et al. Composite mineralized collagen/polycaprolactone scaffold-loaded microsphere system with dual osteogenesis and antibacterial functions. Polymers 2024;16:2394.
[33] Sani IS, Rezaei M, Khoshfetrat AB, Razzaghi D. Preparation and characterization of polycaprolactone/chitosan-g-polycaprolactone/hydroxyapatite electrospun nanocomposite scaffolds for bone tissue engineering. Int J Biol Macromol 2021;182:1638–49.
[34] Krobot Š, Melčová V, Menčík P, Kontárová S, Rampichová M, Hedvičáková V, et al. Poly (3-hydroxybutyrate)(PHB) and polycaprolactone (PCL) based blends for tissue engineering and bone medical applications processed by FDM 3D printing. Polymers 2023;15:2404.
[35] Li R, Xu S, Guo Y, Cao C, Xu J, Hao L, et al. Application of collagen in bone regeneration. Journal of Orthopaedic Translation 2025;50:129–43.
[36] Yang X, Wang Y, Zhou Y, Chen J, Wan Q. The application of polycaprolactone in three-dimensional printing scaffolds for bone tissue engineering. Polymers 2021;13:2754.
[37] Wang W, Zhou X, Yin Z, Yu X. Fabrication and evaluation of porous dECM/PCL scaffolds for bone tissue engineering. J Funct Biomater 2023;14:343.
[38] Jang HY, Shin JY, Oh SH, Byun J-H, Lee JH. PCL/HA hybrid microspheres for effective osteogenic differentiation and bone regeneration. ACS Biomater Sci Eng 2020;6:5172–80.
[39] Niu Y, Du T, Liu Y. Biomechanical characteristics and analysis approaches of bone and bone substitute materials. J Funct Biomater 2023;14:212.
[40] Weisgerber DW, Caliari SR, Harley BAC. Mineralized collagen scaffolds induce hMSC osteogenesis and matrix remodeling. Biomater Sci 2015;3:533–42.
[41] Badar W, Ali H, Brooker ON, Newham E, Snow T, Terrill NJ, et al. Collagen pre-strain discontinuity at the bone—cartilage interface. PLoS One 2022;17:e0273832.
[42] Conceição ALC, Perlich J, Haas S, Funari SS. SAXS-CT: a nanostructure resolving microscopy for macroscopic biologic specimens. Biomedical physics & engineering express 2020;6:035012.
[43] Tcacencu I, Carlsöö B, Stierna P, Hultenby K. Local treatment of cricoid cartilage defects with rhBMP-2 induces growth plate–like morphology of chondrogenesis. Otolaryngology-Head Neck Surg (Tokyo) 2006;135:427–33.
[44] Vidal L, Kampleitner C, Krissian S, Brennan MA, Hoffmann O, Raymond Y, et al. Regeneration of segmental defects in metatarsus of sheep with vascularized and customized 3D-printed calcium phosphate scaffolds. Sci Rep 2020;10:7068.
[45] Liu K, Meng C-X, Lv Z-Y, Zhang Y-J, Li J, Li K-Y, et al. Enhancement of BMP-2 and VEGF carried by mineralized collagen for mandibular bone regeneration. Regen Biomater 2020;7:435–40.
[46] Buss DJ, Kröger R, McKee MD, Reznikov N. Hierarchical organization of bone in three dimensions: a twist of twists. J Struct Biol X 2022;6:100057.
[47] Crovace AM, Lacitignola L, Forleo DM, Staffieri F, Francioso E, Di Meo A, et al. 3D biomimetic porous titanium (Ti6Al4V ELI) scaffolds for large bone critical defect

reconstruction: an experimental study in sheep. Animals (Basel) 2020 Aug 11;10 (8):1389. https://doi.org/10.3390/ani10081389. PMID: 32796533; PMCID: PMC7459697.

[48] Garot C, Schoffit S, Monfoulet C, Machillot P, Deroy C, Roques S, et al. 3D-Printed osteoinductive polymeric scaffolds with optimized architecture to repair a sheep metatarsal critical-size bone defect. Adv Healthc Mater 2023 Dec;12(30): e2301692. https://doi.org/10.1002/adhm.202301692. Epub 2023 Sep 17. PMID: 37655491; PMCID: PMC11468956.

[49] Cipitria A, Wagermaier W, Zaslansky P, Schell H, Reichert JC, Fratzl P, et al. BMP delivery complements the guiding effect of scaffold architecture without altering bone microstructure in critical-sized long bone defects: a multiscale analysis. Acta Biomater 2015 Sep;23:282–94. https://doi.org/10.1016/j.actbio.2015.05.015. Epub 2015 May 22. PMID: 26004222.

[50] Liu X, Li X, Fan Y, Zhang G, Li D, Dong W, et al. Repairing goat tibia segmental bone defect using scaffold cultured with mesenchymal stem cells. J Biomed Mater Res B Appl Biomater 2010 Jul;94(1):44–52. https://doi.org/10.1002/jbm.b.31622. PMID: 20336727.